A Comprehensive Study of Hydrolyzed Polyacrylamide as a Binder for Silicon Anodes

Andrea Miranda,[†] Xiaoyi Li,[‡] Atetegeb Meazah Haregewoin,[§] Kasturi Sarang,[∥] Jodie Lutkenhaus,[*,∥,⊥] Robert Kostecki,[*,§] and Rafael Verduzco[*,‡,#]

[†]Department of Chemistry, Rice University, 6100 Main Street, MS-60, Houston, Texas 77005, United States

[‡]Department of Chemical and Biomolecular Engineering, Rice University, 6100 Main Street, MS-362, Houston, Texas 77005, United States

[§]Energy Storage & Distributed Resources Division, Lawrence Berkeley National Laboratory, 1 Cyclotron Road, Berkeley, California 94720, United States

[∥]Artie McFerrin Department of Chemical Engineering and [⊥]Department of Materials Science and Engineering, Texas A&M University, College Station, Texas 77843, United States

[#]Department of Materials Science and Nanoengineering, Rice University, 6100 Main Street, MS-325, Houston, Texas 77005, United States

ABSTRACT: Silicon anodes have a high theoretical capacity for lithium storage, but current composite electrode formulations are not sufficiently stable under long-term electrochemical cycling. The choice of polymeric binder has been shown to impact stability and capacity of silicon anodes for electrochemical energy storage. While several promising polymeric binders have been identified, there is a knowledge gap in how various physicochemical properties—including adhesion, mechanical integrity, and ion diffusion—impact electrochemical stability and performance. In this work, we comprehensively investigate the physical properties and performance of a molecular-weight series ($3-20 \times 10^6$ g/mol) of partially hydrolyzed polyacrylamide (HPAM) in silicon anodes. We quantify the mechanical strength, electrolyte uptake, adhesion to silicon, copper, and carbon, as well as electrochemical performance and stability and find that HPAM satisfies many of the properties generally believed to be favorable, including good adhesion, high strength, and electrochemical stability. HPAM does not show any electrolyte uptake regardless of any molecular weight studied, and thin films of mid- and high-molecular-weight HPAM on silicon surfaces suppress lithiation of silicon. The resulting composite electrodes exhibit an electrochemical storage capacity greater than 3000 mAh/g initially and 1639 mAh/g after 100 cycles. We attribute capacity fade to failure of mechanical properties of the binder or an excess of the solid electrolyte interphase layer being formed at the Si surface. While the highest-molecular-weight sample was expected to perform the best given its stronger adhesion and bulk mechanical properties, we found that HPAM of moderate molecular weight performed the best. We attribute this to a trade-off in mechanical strength and uniformity of the resulting electrode. This work demonstrates promising performance of a low-cost polymer as a binder for Si anodes and provides insight into the physical and chemical properties that influence binder performance.

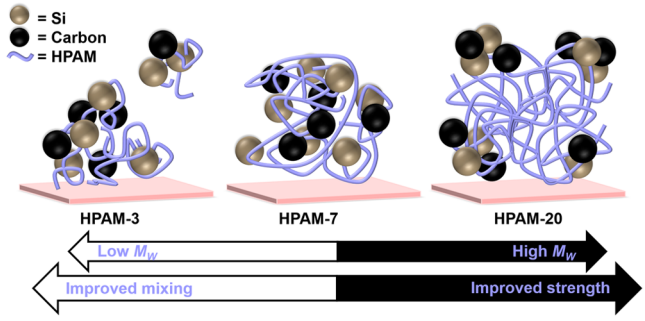

1. INTRODUCTION

Silicon has a theoretical charge capacity for lithium-ion storage of 3579 mAh/g, roughly ten times higher than that of graphite (372 mAh/g).[1] Replacing graphite with silicon could significantly reduce the size of anodes and/or increase the cell energy density. However, current formulations of composite silicon anodes are not sufficiently stable under long-term cycling for practical applications.[2] Failure has been attributed to the large volume changes of silicon particles during charge and discharge, which result in particle disintegration and continuous reformation of the solid electrolyte interphase (SEI) layer, which further aggravates the inherently nonpassivating behavior of Si in organic carbonate electrolytes.[3]

Polymeric binders play a critical role in the electrochemical performance and stability of composite Li-ion electrodes.

Binders in silicon anodes typically comprise more than 10 wt % of the composite electrode and serve multiple functions, which include maintaining the mechanical integrity of the composite electrode, suppressing pulverization of the electrode film, and preventing delamination from the copper current collector. Effective polymeric binders must satisfy a number of properties, including chemical and electrochemical stability within the potential window of electrode operation, strong adhesion to silicon, a high modulus and high elasticity, and, ideally, self-healing behavior, as detailed in a number of reviews on binders for silicon anodes.[4−8] The interaction of the binder with the electrolyte and the amount of swelling or uptake by the binder are also important characteristics that can influence mechanical properties, electrochemical stability, and Li-ion mobility.[9−12] While several promising polymeric binders have been identified, for many of these materials, there is a lack of fundamental understanding in how polymeric binder properties influence performance and how the relationship between various physicochemical properties—including adhesion, mechanical integrity, electrochemical stability, and ion diffusion—determines stability and performance of the silicon anode.

A few recent studies have shown that polyacrylamide (PAM) is a promising binder material for Si anodes. Zhu et al. synthesized a cross-linked PAM network in situ, inspired by the chemistry that produced highly stretchable hydrogel networks. Their work showed that Si anodes with cross-linked PAM as a binder resulted in impressive stability.[13] Yoo et al. also studied a cross-linked PAM network as a binder in Si anodes and found that systematic variations of the cross-link density had a significant impact on performance and stability.[14] While these studies indicate that PAM is a promising material for Si anodes, these studies did not conduct an analysis of various physicochemical properties relevant to battery performance, including adhesion strength, electrolyte uptake, and electrochemical stability. These studies also utilized in situ cross-linking and/or polymerization to produce the binder, which increases the complexity of the electrode fabrication process. Here, we study commercially available samples of partially hydrolyzed polyacrylamide (HPAM) as binders for Si anodes. HPAM is produced industrially at the large scale for enhanced oil recovery applications[15,16] and is a low-cost, widely available material. Partial hydrolysis introduces acrylic acid groups along the polymer chain (molecular structure in the Figure S1, Supporting Information), which enhances stability in oilfield conditions; however, for battery applications, it can potentially improve adhesion to Si, as has been shown in a number of studies with poly(acrylic acid) (PAA) binders.[11,17] One study utilized HPAM in silicon anodes and found low capacities,[18] but here we show that HPAM is an effective binder and can be used to produce electrodes with performance comparable to other state-of-the-art binder materials.

Here, we present a comprehensive study of a series of high-M_w (ranging from 3 to 20 × 10^6 g/mol) HPAM binders to understand the relationship between the physicochemical properties of the polymeric binder and the electrode stability and performance. Our work shows that HPAM satisfies many of the properties generally believed to be favorable, including good adhesion, high strength, and electrochemical stability. The resulting electrodes exhibit an electrochemical storage capacity greater than 3000 mAh/g initially and 1639 mAh/g after 100 cycles. We attribute capacity fade to failure of mechanical properties of the binder or an excess of the solid electrolyte interphase (SEI) layer being formed at the Si surface. The highest-molecular-weight sample exhibited the strongest adhesive forces to silicon and copper and as a result was expected to perform the best. Interfacial adhesion has been cited as a key determinant of good cell cycling in Si anodes.[11,12,19−31] However, we found that HPAM of moderate molecular weight produced more stable and higher capacity electrodes. We attribute this to a trade-off in mechanical strength and uniformity of the resulting electrode. This work demonstrates promising performance of a low-cost polymer as a binder material for Si anodes and provides insight into the physical and chemical properties that influence electrochemical performance.

2. EXPERIMENTAL SECTION

2.1. Chemicals. A series of high-molecular-weight copolymers of partially hydrolyzed polyacrylamide (HPAM, product name FLOPAAM) were sourced from SNF FLOERGER. Three molecular weights were chosen, which we term HPAM-3 (M_w = 3 × 10^6 g/mol), HPAM-7 (M_w = 6−8 × 10^6 g/mol), and HPAM-20 (M_w = 20 × 10^6 g/mol), where the numbers denote the mass averaged molecular weight of each sample. The degree of hydrolysis is 25 mol % for each sample, corresponding to a molar ratio of 75:25−70:30 PAM/PAA repeat units in each polymer. This was confirmed through titration measurements of HPAM solutions (Figure S2, Supporting Information). Poly(vinylidene difluoride) (PVDF, M_w = 534 000 g/mol), lithium polyacrylate (PAALi, M_w = 450 000 g/mol), and *N*-methyl-2-pyrrolidone (NMP) were purchased from Sigma-Aldrich. Poly(1-pyrenemethyl methacrylate) (PPy, M_w = 34 000 g/mol) was synthesized at the Cell Analysis, Modeling and Prototyping facility at Argonne National Laboratory. Silicon nanopowder (50−70 nm, laser synthesized, polycrystalline structure) was purchased from U.S. Research Nanomaterials, Inc., and Super P carbon black (CB, 20−45 nm) was purchased from Alfa Aesar. Lithium foil was purchased from Alfa Aesar. Ethylene carbonate (EC, 99%, Sigma-Aldrich), diethyl carbonate (DEC, ≥99%, Sigma-Aldrich), fluoroethylene carbonate (FEC, ≥99%, Solvay), and lithium hexafluorophospate ($LiPF_6$, ≥99.99%, Sigma-Aldrich) were used to prepare 1 M $LiPF_6$ in EC/DEC (1:1 v/v) with 10 wt % FEC electrolyte solution. Glass fiber separators (Whatman) were used in model electrode cell testing. For the composite cell testing, the electrolyte was sourced from BASF with the same composition as mentioned above, and polypropylene separators were provided by Celgard (3501).

2.2. Composite Electrode Fabrication. A slurry composed of 70:15:15 Si/CB/HPAM in Millipore water was prepared by mixing all components in a planetary mixer (ARE-310, Thinky). The slurry concentration was 80 mg/mL, and the contents were mixed for 4 min at 1500 rpm, providing 3 min rest intervals to prevent overheating, for a total of 60 min of mixing time. The slurry was then placed in a vacuum chamber for 5−10 min to degas before coating, stirred briefly, and then cast onto copper foil using a home-built flow coater[32] with a gap height of 100 μm. The cast films had a thickness of 20 μm after drying and dimensions of 15 cm × 5 cm. Films were dried in a fume hood overnight, punched for testing in coin cells, and subsequently dried in a vacuum chamber at 70 °C for 15 h. Electrodes with a diameter of 16 mm and a total mass loading of 1 mg/cm^2 (Si mass loading 0.7 mg/cm^2) were assembled in a glovebox filled with Ar with <0.1 ppm H_2O and O_2. Notably, the viscosity of polymers reduced after planetary mixing, indicating some polymer chain rupture during blending. However, the measured viscosity after blending still trends with molecular weight, with HPAM-20 having the highest viscosity and HPAM-3 the lowest (see the Table S1, Supporting Information).

2.3. Model Electrode Fabrication. Model Si electrodes were composed of 500 μm-thick B-doped p-type Si(100) wafers with 0.001 Ω cm resistivity and were sourced from MTI. B-doped Si wafers rather than undoped Si were used because undoped Si wafers are nonconductive. The B content of these Si wafers is low

(approximately 9 boron atoms per 10 000 silicon atoms),[33] and therefore we do not expect that this will significantly impact electrochemical behavior. Model copper electrodes were composed of Si wafers coated with an adhesive 3 nm-thick chromium sublayer and topped with a 100 nm thermally evaporated copper film. Thin films of hydrolyzed polyacrylamide were deposited on the wafers using a spin-coater (Specialty Coating Systems, Spincoat G3P-8) after treating the wafers with a Jelight model 42 UVO cleaner for 15 min. Then, 0.25 wt % solutions of the three variants of hydrolyzed polyacrylamide in Millipore water were cast at 3000 rpm for 90 s. UV−ozone (UVO) surface treatment was necessary to deposit uniform films on the surface by spin-coating; the solutions and films dewet from the untreated surface. Samples were dried overnight at room temperature and further dried at 70 °C for 15 h under vacuum and directly transferred to a glovebox filled with Ar with <0.1 ppm H_2O and O_2. Atomic force microscopy was used to measure the thickness of the polymer film on the wafer. The step height of a scratch made on the film was 18.2 ± 2 nm for the HPAM-3 film, 16.3 ± 2.1 nm for the HPAM-7 film, and 15.1 ± 0.4 nm for the HPAM-20 film (Figure S3, Supporting Information). Micrographs of polymer-coated Si wafers confirmed film uniformity, with no pinholes or other nonuniformities on the surface (inset of Figure S4a−d, Supporting Information). The calculated polymeric binder coating thickness on a Si nanoparticle in a composite electrode in our system was around 20 nm assuming uniform coverage.[34] Pristine and HPAM-coated wafers were cut to 0.8 × 0.8 cm^2 squares prior to testing.

2.4. Electrochemical Testing. Model electrodes were assembled in a three-electrode stainless steel Swagelok "Tee" cell. The pristine and polymer-coated wafers were used as working electrodes, while lithium foil was used as both the counter and reference electrodes. The wafer electrodes were surrounded by Torr Seal epoxy to avoid electrolyte penetration along the uncoated edges and backside of wafers. In a typical cell, 10 μL of electrolyte was dropped between the Si working and Li-foil counter electrode, and 20 μL of electrolyte was dropped on the reference electrode separators. Two glass fiber separators were placed between the working and counter electrodes and two in front of the reference electrode. Cyclic voltammetry (CV) was collected at a scan rate of 0.1 mV/s for 10 cycles with a VMP3 multichannel potentiostat (Bio-Logic Science Instruments). The scanning potential range for all electrodes was set from 1.5 to 0.01 V vs Li/Li^+.

Coin cells (CR2032) were composed of a Si working electrode and a Li-foil counter electrode separated by two Celgard separators wet with 20 μL of electrolyte. Cells were cycled at a constant current−constant voltage (CC−CV) mode for the initial five formation cycles (at the end of each lithiation, the voltage was held at 0.01 V until the current decreased to 0.15 mA). The cycling rate was set to C/10 for both the CC−CV cycles and following cycles. Current values were calculated based on the mass of Si in the electrode. Analyzed samples were rinsed with DEC for 5 s and dried in a glovebox overnight for further analysis. Composite electrodes were collected for post mortem scanning electron microscopy (SEM) analysis after 275 cycles or until cells exhibited no measurable current.

2.5. Mechanical Testing. Adhesion measurements were performed on a Chatillon TCD225 Series Digital Force Tester. Samples were prepared by drop-casting 10 μL of saturated polymer solution in H_2O (HPAM, PAALi) or NMP (PPy, PVDF) on a substrate (Si wafer, Si/Cu wafer, or glassy carbon (Alfa Aesar)) and then placing another substrate on top to sandwich the binder between two substrates. For water-based solutions, substrates were treated in a UV ozone cleaner for 15 min prior to drop-casting to improve spreading of the solution on hydrophobic surfaces. Sandwiched samples were pressed with a force of 0.2 N and dried overnight at room temperature, followed by further drying at 70 °C for 15 h under vacuum. These drying conditions were chosen to stay consistent with the processing conditions of the composite electrodes. For comparison, adhesion tests were also performed on samples after only drying at room temperature. A schematic of the configuration is shown in the Supporting Information (Figure S5). The sample was pulled apart at a rate of 3 mm/min until separated at the polymer−substrate interface or until maximum tension was reached. Failure in all cases was due to adhesive failure of the binder at the interface.

Tensile tests on HPAM variants were performed using an ARES G2 rheometer (TA Instruments). Films were prepared by drop-casting 12.5 mg/mL solution of HPAM in H_2O onto polystyrene weigh boats and dried at room temperature overnight. The samples were cut into rectangles of 5 × 20 mm^2 with a thickness of approximately 0.03 mm. Linear tension was applied to the samples at a strain rate of 0.05% of the sample length per second until failure.

Viscosity measurements were done on a Brookfield viscometer from a 12.5 mg/mL HPAM solution in water (the concentration of binder in water used in slurry preparation).

2.6. Binder Swelling Characterization. To determine chemical reactivity and electrolyte uptake of HPAM, swelling tests were performed on the pristine HPAM polymer powder and the HPAM polymer powder after soaking in the electrolyte. These two samples were compared by thermogravimetric analysis (TGA) and attenuated total reflectance Fourier transform infrared (ATR-FTIR) spectroscopy. TGA was carried out on Q-600 Simultaneous TGA/DSC (TA Instruments). ATR-FTIR spectroscopy was collected inside an environmental chamber (818GBB/Plaslabs) filled with N_2. A Shimadzu IRTracer-100 spectrophotometer outfitted with single reflection PIKE technologies MIRacle ATR sampling accessory equipped with a Ge crystal was used to record ATR-FTIR spectra. The spectra were accumulated over 128 scans with a spectral resolution of 4 cm^{-1}. Baseline corrections were performed in OriginPro software. Powdered samples of HPAM were dried at 70 °C for 15 h under vacuum before soaking because the polymer contained water without the drying step, as determined by TGA. Roughly 200 mg of powder was soaked in 5 mL of electrolyte for 24 h and then filtered and rinsed with DEC. The powder was left to dry for 36 h in the glovebox. TGA sample sizes were between 5 and 10 mg, which were heated in alumina crucibles under flowing N_2 (100 mL/min) at a rate of 10 °C/min from room temperature to 800 °C. FTIR spectra were collected on the pristine and soaked polymer powders.

2.7. Spectroscopic and Microscopic Characterization. X-ray photoelectron spectroscopy (XPS) was acquired using a PHI Quantera X-ray photoelectron spectrometer. The spot size, energy step, and pass energy were 200 μm, 0.2 eV, and 55 eV, respectively. The data were shifted based on C 1s peaks shifted to 284.8 eV, the C═O peak at 532 eV, the Si−O peak at 103.1 eV, or the Si 2p is peak at 99.4 eV.

Scanning electron microscopy (SEM) was used to observe the morphology of model electrodes before and after cycling. The images were collected at 5 kV on a JOEL SEM (JSM-6700F). SEM images of the composite electrodes before and after cycling were collected on an FEI Quanta 400 ESEM FEG. All cycled electrodes were rinsed with DEC briefly before imaging.

3. RESULTS AND DISCUSSION

3.1. Chemical and Mechanical Properties of Binders. The analysis of polymeric binders was focused on a series of partially hydrolyzed polyacrylamide (HPAM) polymers, random copolymers of acrylamide, and acrylic acid [see the Figure S1 (Supporting Information) for the molecular structure of the polymer]. We hypothesized that very high molecular weights of the polymers would result in mechanically robust and stable electrodes and that cycling stability would improve with increasing molecular weight. To test this, we conducted a comprehensive analysis of adhesion, tensile strength, viscosity, electrolyte uptake, and electrochemical stability of HPAM.

To evaluate the adhesion of polymeric binders to silicon, carbon, and copper, we measured the force required to pull apart two pieces of either material held together by a layer of polymeric binder. We tested each HPAM binder along with other polymers used in silicon anodes: poly(1-pyrenemethyl

methacrylate) (PPy), lithium polyacrylate (PAALi), and poly(vinylidene difluoride) (PVDF). The results for binding force are reported in Figure 1 for samples dried at room temperature overnight followed by 70 °C under vacuum for 15 h.

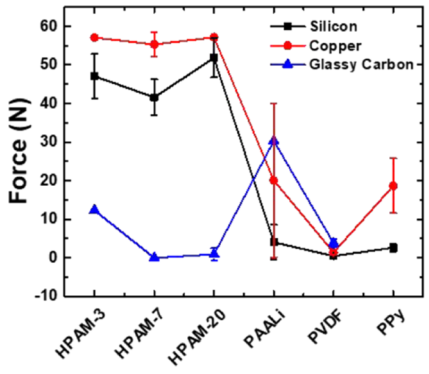

Figure 1. Force required to pull apart silicon (black square), copper (red circle), or glassy carbon (blue triangle) substrates using various binders drying at 70 °C under vacuum. (PPy was not tested on glassy carbon because it typically is not mixed with a carbon additive in composite electrodes.) Lines are used to guide the eye for comparison.

HPAM exhibits superior adhesion to silicon and copper compared with PAALi, PPy, and PVDF binders, and the adhesion is the strongest for HPAM-20. This strong adhesion of HPAM to silicon and copper is attributed to the polarity and relatively high molecular weight of the HPAM polymers tested.[35] Polymers with polar hydroxyl and/or carboxylic acid groups have been shown to adhere more strongly to silicon in comparison with hydrophobic polymers like PVDF.[8,36] Conversely, as shown in Figure 1, the adhesion of all HPAM binders to carbon is relatively weak, which may be attributed to the hydrophobic nature of the carbon substrate.[8]

The data shown in Figure 1 are for binders annealed at 70 °C under vacuum, which are the conditions used to prepare electrodes. For comparison, we also investigated polymeric binders dried under ambient conditions (see the Table S2, Supporting Information). All three variants of HPAM exhibit superior adhesion when dried at room temperature. The same trends are observed in the HPAM binders as the samples dried at 70 °C: they exhibit stronger binding to silicon and copper than glassy carbon and stronger binding with increasing molecular weights. For the other binders tested, PAALi shows comparable binding force to HPAM when dried at room temperature, and PVDF shows strong adhesion to silicon and carbon but not to copper. PPy demonstrates relatively poor adhesion to the three substrates. PAALi and PVDF also show poorer adhesion after annealing, although PAALi is found to have the strongest binding to carbon among all binders tested after annealing at 70 °C. PPy exhibited poor adhesion under both conditions, but the adhesion did improve on annealing at 70 °C, in agreement with a previous work.[19] We also note that these measurements are conducted on dry polymeric binders in contact with different surfaces. As discussed below, the HPAM binders do not significantly uptake electrolyte, and therefore these measurements likely capture the relevant adhesive forces in nanocomposite electrodes. For binders such as PAA or PAALi, which swell in electrolyte and exhibit excellent performance in nanocomposite electrodes,[37] dry adhesion measurements may not accurately reflect the adhesion forces in the presence of electrolyte.

The mechanical strength of the binders was examined using tensile strength testing. Pure polymeric binders cut into rectangular strips and dried were stretched uniaxially until failure (Figure S6a). The measurements indicated that all three HPAM samples had a similar modulus and that the failure stress and strain increased with molecular weight. HPAM-20 exhibited failure at 74 MPa and 3.4% strain, HPAM-7 at 32 MPa and 0.9% strain, and HPAM-3 at 27 MPa and 1.0% strain, indicating an improvement in tensile strength with increasing molecular weight. The moduli and maximum tension achieved for each MW are plotted in Figure S6b.

To test for electrolyte uptake, HPAM films were soaked in electrolyte for 24 h and then removed and patted dry; the mass was then measured before and after drying. No detectable change in mass was observed after soaking in electrolyte. Electrolyte uptake of the polymer binders was also tested by soaking dried polymer granules in electrolyte, filtering, rinsing, drying, and then comparing the pristine samples to the soaked samples using FTIR spectroscopy and TGA, following a method recently applied to study pyrenemethyl methacrylate (PPy) binders (Figure 2).[19] The FTIR spectra (Figure 2a) do

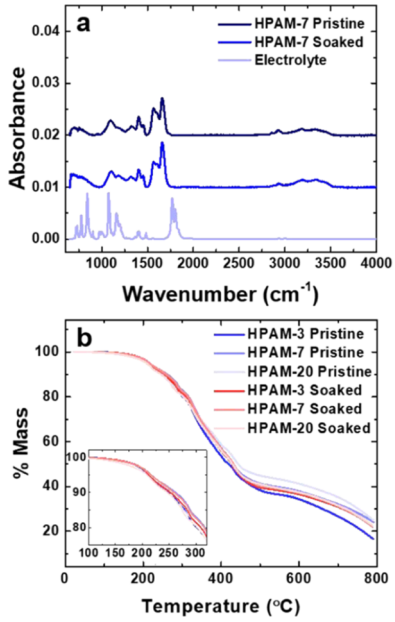

Figure 2. FTIR spectra before and after soaking the HPAM-7 in electrolyte (a). TGA curves of HPAM before and after soaking in electrolyte (b). Inset shows a zoomed-in portion of (b) and demonstrates overlap of the TGA curves.

not show any noticeable changes after soaking in the electrolyte. The C–N peak at 1416 cm^{-1}, N–H peaks at 1617, 3200, and 3348 cm^{-1}, and the C═O peak at 1661 cm^{-1} are all indicative of HPAM and indicate that HPAM remains unchanged after soaking in electrolyte.[38] Absence of IR bands characteristic of the electrolyte in the FTIR spectra also indicates that electrolyte solvents are not trapped within the polymer after soaking and drying. These results are also consistent with TGA analysis (Figure 2b). If any electrolyte solvents were trapped in the polymer matrix, these would be observed as a mass loss at temperatures near the boiling points of the electrolyte components EC, DEC, and FEC, which are

243, 127, and 212 °C, respectively. In fact, no change in mass loss is observed at these temperatures for any HPAM polymeric binder. This contrasts with similar tests performed on PPy, which showed evidence of electrolyte uptake by FTIR and TGA even after washing the binder.[19]

3.2. Electrochemical Measurements of Model Si Electrodes and Surface Microscopy. To test the electrochemical stability of the binders, cyclic voltammetry studies were conducted on Si/HPAM and Cu/HPAM model electrodes, which consisted of uniform thin polymeric binder films (20 ± 10 nm) on Si and Si/Cu wafers. These model electrodes enable us to isolate electrochemical activity at the Si/polymer and Si/electrolyte interfaces. We note that both of these interfaces are relevant to the electrode devices as the polymeric binder likely does not uniformly coat the nanoparticle surfaces. Cyclic voltammograms (CVs) of bare Si and HPAM-coated Si of different molecular weights are shown in Figures 3, S7, and S8 and were performed in the voltage range

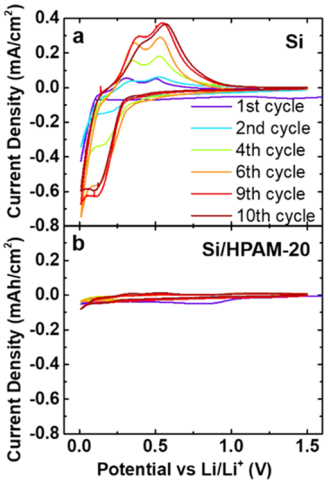

Figure 3. Cyclic voltammogram of model electrodes on Si from 0.01 to 1.5 V vs Li/Li^+ for 10 cycles at a rate of 0.1 mV/s (a, b). For clarity, only Si and Si/HPAM-20 are shown here, and Si/HPAM-3 and Si/HPAM-7 are shown in Figure S7, Supporting Information.

of 0.01−1.5 V at a scan rate of 0.1 mV/s. The CV trace on bare silicon (Figure 3a) shows expected behavior with distinct lithiation and delithiation peaks. Expanded CV traces clearly show four cathodic peaks and two anodic peaks in the first cycle (Figure S8, Supporting Information). FEC decomposition occurs first, marking the onset of electrolyte decomposition.[39] Further electrolyte decomposition peaks appear at 1.39 and 0.52 V, corresponding to reduction of DEC and EC, respectively.[40,41] The small peak at 0.28 V has been attributed to lithiation of crystalline Si,[42] and the sharp peak starting at 0.10 V represents the lithiation of amorphous Si.[43] Two delithiation peaks are present at 0.31 and 0.50 V. Starting at the second cycle, the Si lithiation peak shifted to ∼0.30 V. Similarly, the delithiation peaks shifted to 0.35 and 0.53 V. The peak shifts in the cathodic and anodic scans may indicate formation of a solid electrolyte interphase (SEI) layer, phase transformation, or increased kinetic polarization and internal resistance.[44,45] By the 10th cycle (Figure 3), the delithiation peaks merged. The CV traces in Figure 3a show increased current density in the lithiation peak with increased cycling as fresh Si surfaces are exposed as a result of volumetric expansion and contraction. An SEI layer capable of mitigating electrolyte reduction does not form on the silicon surface, resulting in the unencumbered increasing current density of the lithiation peak.

In contrast to the Si electrode, the CV of Si/HPAM-3 does not exhibit a strong lithiation peak (Figure S7a, Supporting Information), indicating that HPAM-3 acts as a barrier between Li ions and Si. In the first cycle (Figure S8b, Supporting Information), a new peak at 1.7 V appears. Two broad peaks are apparent centered at 1.25 and 0.50 V, with a sharp, if small, lithiation peak starting at 0.10 V. Delithiation peaks are clearly visible at 0.55 and 0.31 V. In the second cycle, the broad peak at 1.25 V reappears, shifted slightly to 1.33 V. The lithiation peak appears starting at 0.28 V, but it increases in current density from the first cycle. Two delithiation peaks are clearly visible at 0.37 and 0.55 V. By the third cycle, the lithiation peak onset shifted to 0.42 V. From these results, we conclude that HPAM-3 slightly hinders lithium ions from reacting with the silicon surface underneath; however, the characteristic lithiation peaks are visible starting from the first cycle. Also, the electrolyte decomposition peaks are still present in the first cycle, indicating that electrolyte may be forming an SEI layer on the electrode.

The CV traces of Si/HPAM-7 (Figure S7b, Supporting Information) and Si/HPAM-20 (Figure 3b) show even lower current densities and less overall charge consumed than Si/HPAM-3 in both the electrolyte reduction potential regions and the lithiation potential region, indicating that the binder significantly inhibits the diffusion of lithium ions to the silicon. Still, some electrochemical activity was detected. In the expanded Si/HPAM-7 CV trace (Figure S8c, Supporting Information), cathodic peaks are visible at 1.30 and 0.55 V corresponding to the electrolyte decomposition, and a small lithiation peak is visible starting at 0.12 V. One anodic peak is visible at 1.06 V. Upon further cycling, the electrolyte decomposition peaks are reduced and shifted slightly to 1.36, 0.67, and 0.34 V. The Si/HPAM-20 CV trace shows cathodic peaks similar to those of Si/HPAM-7 at 2.46, 1.30, and 0.83 V. A lithiation peak begins at 0.08 V, and two delithiation peaks are visible at 0.32 and 0.53 V. As with Si/HPAM-7, upon further cycling, the electrolyte decomposition peaks are reduced and shifted slightly to two broad peaks at 1.36 and 0.67 V and two sharper peaks at 0.37 and 0.15 V.

These studies show that HPAM films reduce electrochemical activity at the surface of Si, likely due to the very low degree of electrolyte uptake in these materials. While this may appear to be an undesirable property for a polymer binder, we note that many of the best polymeric binders for silicon nanocomposite electrodes exhibit similar properties. For example, alginate polymer was found to exhibit no measurable electrolyte uptake, and it blocked the electrolyte from reaching the silicon surface. The authors concluded that this was an important property to maintain strong adhesion of the binder to the silicon nanoparticles.[9] Another study similarly reported no swelling in poly(acrylic acid) (PAA) binders.[11] Additionally, a recent study demonstrated that PAA and sodium carboxymethyl cellulose (CMC) improved electrochemical stability by preventing electrolyte decomposition at the silicon surface.[46] We also note that some electrochemical activity is observed in model electrodes with thin HPAM films, and the electrochemical activity measured in HPAM-coated model Si electrodes decreases with increasing HPAM molecular weight.

Finally, CVs of model Cu electrodes are shown in the Figure S9, Supporting Information. These are used to indicate electrochemical stability of HPAM. Peak heights are greatly

reduced compared with Si model electrodes, and CV traces indicate that there may be only minor oxidation−reduction reactions involving the electrolyte or HPAM, electrolyte decomposition, or HPAM decomposition contributing to the electrochemistry of the Si model electrodes. These results indicate good electrochemical stability of HPAM within the operating voltage window.

The surface morphology of the Si/HPAM model electrodes was analyzed before and after cycling by SEM. The surfaces of the pristine electrodes are shown in the inset images in the Figure S4 (Supporting Information) and are smooth and featureless, as expected for a uniform spin-coated HPAM thin film on a Si wafer. After electrochemical cycling, the surface of the Si/HPAM model electrodes shows small and large agglomerates of the electrolyte decomposition products. Consistent with the electrochemical data, increasing the molecular weight of HPAM appears to inhibit the interaction of the Si with the electrolyte and formation of the SEI layer on the electrode surface. Lithium diffusion in polymer electrolytes occurs through a hopping mechanism dependent on segmental dynamics and therefore should be molecular-weight independent.[47] However, our results clearly indicate a molecular-weight dependence of electrochemical activity. We do not fully understand this molecular-weight dependence but propose that this may be due to differences in electrolyte uptake or mobility among the polymer samples, with higher electrolyte mobility in the low-molecular-weight HPAM. Another work has indicated that ionic conductivity could be compromised with use of higher-molecular-weight binders due to a greater surface area coverage of the active material by the longer chain lengths.[9,48,49] Less surface coverage is deemed more beneficial because ionic conductivity is higher in the electrolyte than in the binder.

3.3. Ex Situ Spectroscopic Surface Analysis. To gain more insight into the surface chemistry of the model electrodes and to study the stability of HPAM, XPS was used to probe the composition of the model electrodes before and after cycling (Figure 4) for only Si/HPAM-3 model electrodes. Additional O 1s and N 1s spectral regions are shown in the Figure S10, Supporting Information. The XPS of the pristine Si/HPAM-3 electrode shows a strong peak at 99.4 eV that corresponds to Si (Figure 4b). The presence of Si−O on the Si wafer surface is identified by the O 1s peak at 532.5 eV (Figure S10a, Supporting Information) and the Si 2p peak at 103.5 eV (Figure 4b). The adventitious carbon C 1s peak is also present at 284.8 eV as expected. The pristine Si/HPAM-3 sample is composed of mainly carbon (Figure 4a), oxygen (Figure S10a, Supporting Information), and nitrogen-containing (Figure S10b, Supporting Information) species, along with some silicon detected in the Si 2p region. The carbon peak is composed of C−H species detected at 284.8 eV and CO_2 at 289 eV.[19] Importantly, no nitrogen peak is observed in Figure S10b (Supporting Information) for the pristine Si, meaning that we can use the presence of a N 1s peak to identify the presence of HPAM-3 on the electrode.

Spectra of the cycled Si and Si/HPAM-3 electrodes were collected before sputtering (0 min) and after sputtering for 16 min to penetrate below any SEI film or electrolyte decomposition products that may have formed on the surface (Figures 4c−f and S10c−f, Supporting Information). The second row shows results from the cycled Si model electrode surface and reveals SEI formation. Figure 4c shows that the Si surface has a variety of carbon species, in contrast to the single

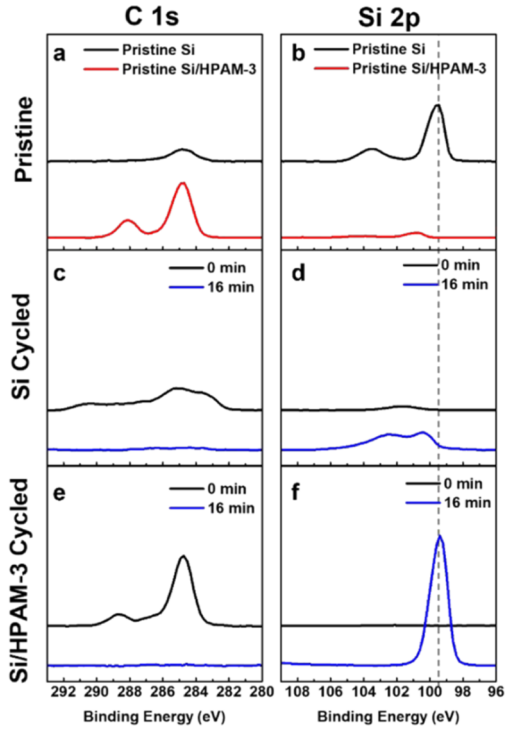

Figure 4. XPS spectra of Si and Si/HPAM-3 model electrodes before cycling (a, b). The second row shows spectra of the cycled Si model electrode (c, d). The third row shows spectra of the cycled Si/HPAM-3 (e, f). Spectral regions are organized by columns signifying C 1s and Si 2p regions for the different samples. Sputter times applied to the samples are listed in legends of plots in the second and third rows. The gray dashed line highlights the Si 2p peak at 99.4 eV for comparison among samples. Additional spectral regions (O 1s and N 1s) are shown in the Figure S10, Supporting Information.

C 1s peak of the pristine Si sample. The carbon peaks are mostly like carbonate species that have formed on the Si surface because of electrolyte decomposition.[50] As the sample is sputtered, the carbon peaks decrease in intensity and the Si peaks increase in intensity.

In the case of the model Si/HPAM thin-film electrode, XPS reveals the formation of an SEI layer and the surface covered with HPAM, which suggests stability of the HPAM binder under cycling. Figures 4e,f and S10e,f (Supporting Information) indicate that the surface of the electrode is still covered by the HPAM as reflected in the C 1s and N 1s spectra. However, the ratio of the C−C (285 eV) to C═O (289 eV) peaks changed from 3:1 to 6:1 after cycling, reflecting the presence of some electrolyte decomposition products formed on the surface of HPAM. The small peak observed in Figure 4b on Si/HPAM-3 also disappears in Figure 4f at 0 min of sputtering, indicating the presence of some additional surface film on top of HPAM. Figure 4f reveals the presence of pristine silicon underlying the SEI and HPAM layers after 16 min of sputtering. This indicates that the HPAM binder has suppressed lithiation of Si on the electrode surface or produced a stable SEI layer on the surface of the electrode, consistent with the cyclic voltammetry studies detailed above on model thin-film electrodes and reflecting good electrochemical stability of the HPAM binder on the Si surface.

3.4. Electrochemical Testing of Composite Si/HPAM Electrodes. The series of HPAM binders were tested through analysis of their performance in Si composite anodes in lithium

metal half-cells. As shown in Figure 5a, the HPAM series produced anodes with initial capacities near 3000 mAh/g,

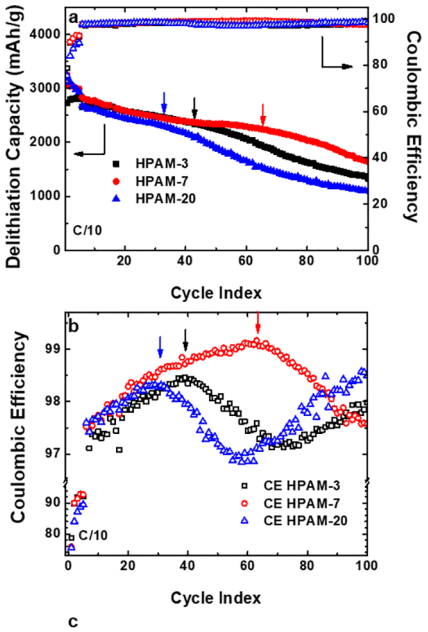

c

Binder	Discharge capacity (mAh/g)	
	5 cycles	100 cycles
HPAM–3	2811	1353
HPAM–7	2988	1639
HPAM–20	2937	1099

Figure 5. Charge–discharge capacities (a) and Coulombic efficiencies (CEs) (b) for half-cell batteries with composite silicon anodes. Table comparing discharge capacity at 5 and 100 cycles (c).

which compares favorably with a variety of polymeric binder materials.[6,8,51,52] The capacity also drops during cycling, but the storage capacity after 100 charge–discharge (from 0.05 to 1.0 V, C/10 or 0.358 A/g) cycles remains near 1640 mAh/g for HPAM-7, which also compares favorably with other polymer binder materials. For example, in a recent study using cross-linked PAM as binders (synthesized in situ), Zhu et al. reported an initial discharge capacity as high as 3000 mAh/g at C/10 for similar electrode and silicon loadings.[13] Similarly, Karkar et al. reported discharge capacities of approximately 2000 and 2500 mAh/g for Si anodes with CMC and PAA binders, respectively, after 50 charge–discharge cycles while cycling at C/7.5 and Si mass loading of 1 mg/cm^2.[17] Bie et al. reported a discharge capacity of 1800 mAh/g after 100 charge–discharge cycles at a lower loading capacity of 0.5 mg/cm^2 Si while cycling at C/2.5 assuming a theoretical capacity of 3579 mAh/g (1.5 A/g).[53] Kovalenko et al. reported a discharge capacity of approximately 1800 mAh/g for alginate binders after 100 charge–discharge cycles at a rate of 4.2 A/g.[9] Lopez et al. reported a discharge capacity of approximately 1500 mAh/g at 100 cycles for Si anodes with supramolecular binders using a mass loading of 0.75–1.1 mg/cm^2 and a rate of C/10.[54] Other examples for comparison have been provided in recent reviews.[4–8,55–57]

The first five cycles in the capacity plot (Figure 5a) are the formation cycles, collected at constant current–constant voltage (CC–CV). The remaining capacity is measured at a rate of C/10. The initial cycles following the formation cycles remain relatively steady but decay at a linear rate of approximately 5 mAh/g per cycle. However, each sample eventually undergoes an accelerated decrease in capacity, indicated by the arrows in Figure 5. Notably, the highest molecular-weight binder, HPAM-20, exhibits the poorest performance, contrary to our expectation that performance would improve with molecular weight. The best stability and performance are exhibited by HPAM-7. We tested the performance of this electrode at varying C-rates, and, as expected, the capacity drops with increasing C-rate (see Figure S11, Supporting Information). This is similar to other studies that have investigated the rate-dependent capacity in silicon nanocomposite anodes.[58]

The point of cell capacity fade is also evident as a peak in the charge/discharge Coulombic efficiency, which coincides with observation of the accelerated decrease in cycling capacity. The peak occurs approximately at 41, 66, and 31 cycles for HPAM-3, HPAM-7, and HPAM-20, respectively. The onset of capacity fade in Si electrodes reflects active material being isolated from the electronic network[59–61] and can be attributed to the failure of mechanical properties of the binder or an excess of the solid electrolyte interphase (SEI) layer being formed at the Si surface. Poor binder integrity results in inhibited electron transport to and from the reaction site. Likewise, the formation of a thick SEI layer can block Li-ion transport to the Si surface. Before the capacity fade, unexposed Si surfaces may have been continuously exposed to electrolyte and lithium ions with every cycle, but at some point, either the unexposed Si was consumed or the SEI layer grew too thick to access the silicon. A closer look at the Coulombic efficiency (CE) in Figure 5b shows that it is less than 100%, indicating that there is a decrease in delithiation capacity. This could occur due to consumption of Li ions in side reactions with the electrolyte or rupture in the electronic network at the silicon–binder–carbon interface.

SEM images of the composite electrode before and after cycling are shown in Figure 6. The pristine samples are

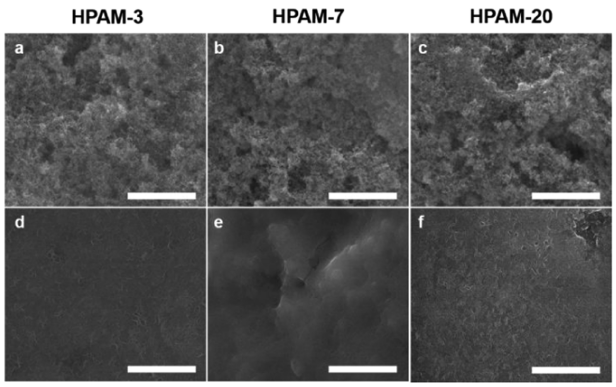

Figure 6. SEM images of the composite electrode surface before (a–c) and after (d–f) cycling. All scale bars are 5 μm in length.

uniformly porous with pores on the micron and submicron scales. The SEM micrographs taken after cycling for 275 cycles show a thick film that uniformly covers the surface of the electrode. This reflects the formation of a solid electrolyte interface (SEI) layer that masks the porous structure of all of the pristine samples. The formation of a thick SEI layer is consistent with the observed decrease in Coulombic efficiency after 31–66 cycles and might be attributed to excessive consumption of Li ions in the formation of the thick SEI layer

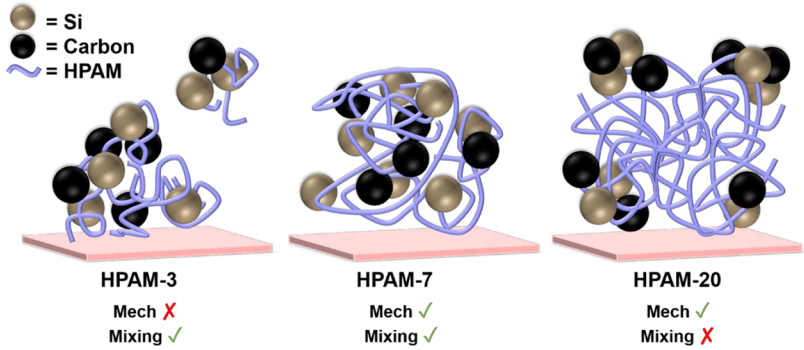

Figure 7. Schematic depicting incorporation of silicon and carbon particles into the polymer matrix of varying molecular weights. The substrate below the polymers represents copper foil. The schematic is not to scale but meant to provide a qualitative representation of the distribution of silicon and carbon nanoparticles and the role of the size of the polymeric binder.

or isolation of Si particles from the electronic network. Cross-section images of the composite electrodes and more images of the cycled composite electrode surfaces are shown in the Figures S12 and S13 (Supporting Information), respectively.

4. DISCUSSION

A systematic analysis of slurry viscosity, polymeric binder mechanical properties, adhesion force, electrolyte uptake, electrochemical activity, and morphological changes provided a detailed picture of the physical properties and performance characteristics of silicon anodes with HPAM binders. This analysis indicated that across the molecular-weight series of HPAM binders, electrolyte uptake was negligible, and adhesion and mechanical strength increased with increasing molecular weight, as hypothesized. Electrochemical activity was suppressed more strongly in model electrodes with high-molecular-weight binders, indicating that HPAM can suppress electrochemical activity at the surface of Si nanoparticles by blocking access to the silicon surface, as has been observed in other effective binder materials for Si anodes.[9] Overall, HPAM exhibits a number of favorable properties as a binder, including adhesion, mechanical strength, and electrochemical stability.

The performance of Si anodes with the HPAM binder is the most impressive with HPAM-7, and those electrodes exhibit an initial capacity of approximately 3000 mAh/g, which decays to 1639 mAh/g after 100 cycles. These discharge capacities compare favorably with other binder materials developed for Si anodes. For example, in one study, a Si anode with 76% Si powder, 12% ultrathin graphite platelets, 12% poly(acrylic acid) (PAA, 450 000 g/mol) binder, and a Si mass loading of 1 mg/cm^2 had an initial capacity slightly above 3500 mAh/g, and after 50 cycles, the capacity was slightly above 2500 mAh/g when cycled at a rate of C/7.5.[17] In comparison, at 15% HPAM, a rate of C/10, a mass loading of 0.7 mg$_{Si}$/cm^2 and after 50 cycles, HPAM-7 has a capacity of 2300 mAh/g.

However, we clearly observe capacity fade in all anodes tested, and the capacity fade initiates the most rapidly in electrodes with HPAM-20, the highest molecular-weight binder studied. The most stable electrode performance was observed with a binder of moderate molecular weight, HPAM-7. This result reflects tradeoffs in properties of the binder with increasing molecular weight and highlights the complexity of optimizing polymeric binders for Si anodes, which must simultaneously perform a variety of functions. While adhesion strength and mechanical properties are improved with increasing molecular weight, the slurry viscosity is also increased. This may lead to poor mixing and dispersion of the conductive additive and silicon particles, resulting in a poorly dispersed conductive phase, as shown schematically in Figure 7.

Previous work has investigated the properties of poly(1-pyrenemethyl methacrylate) (PPy) as a binder for silicon anodes and found that it preferentially took up DEC in the electrolyte.[19] PPy allowed Li-ion mobility through the binder, but the electrolyte uptake also led to electrolyte decomposition at the silicon surface. In the HPAM system, we observe no electrolyte uptake, which may reduce electrolyte decomposition, but this also hinders Li-ion transport to the Si interface. Thus, failure occurs in both HPAM and PPy binder systems, and the analysis conducted in this study along with the previous study on PPy indicates that the reasons for failure are distinct. Processing likely plays an important role, and modifications of the procedure for blending, casting, and postprocessing treatment (such as aging in a humid environment) can potentially enhance stability and discharge capacities.[17]

5. CONCLUSIONS

We comprehensively investigated the physical properties and performance of a molecular-weight series (3−20 × 10^6 g/mol) of partially hydrolyzed polyacrylamide (HPAM) in silicon anodes and found that HPAM satisfies many of the properties generally believed to be favorable, including good adhesion, high strength, and electrochemical stability. The resulting composite electrodes exhibit an electrochemical storage capacity greater than 3000 mAh/g initially and 1639 mAh/g after 100 cycles. In addition to demonstrating the favorable performance of HPAM as a binder for silicon anodes, we found tradeoffs in the properties that exist among the different molecular weights of HPAM tested. HPAM is not chemically reactive with the electrolyte, but with increasing molecular weight, the viscosity increases, the adhesion to silicon increases, the tensile strength increases, and the reactivity on the silicon surface is further suppressed. Slow growth of the SEI layer is observed from the CV data, SEM morphology images, and XPS depth profiling for all Si/HPAM model electrodes. These data also reveal that the rate of the SEI layer growth is reduced on the higher-molecular-weight HPAM. The suppression of the SEI layer formation is beneficial because it avoids uncontrolled growth that could block access to Si. The best capacity retention in composite electrode testing was achieved with HPAM-7, which had an intermediate molecular

weight of the samples tested. We propose that an optimal combination of the viscosity and mechanical strength may have contributed to HPAM-7 exhibiting the highest capacity retention. The increased viscosity of HPAM-20 may inhibit homogeneous distribution of the particles in the slurry, but the decreased mechanical strength of HPAM-3 may rupture sooner under the stress of silicon's volume changes. This combination of beneficial and detrimental properties likely led to HPAM-7 being the optimal-molecular-weight HPAM to use in the composite electrode.

■ ASSOCIATED CONTENT

Supporting Information

The Supporting Information is available free of charge on the ACS Publications website at DOI: 10.1021/acsami.9b13257.

Molecular structure of HPAM, viscosity data, thin-film thicknesses, tabulated adhesion data, tensile testing data, further electrochemical analysis, and further SEM images (PDF)

■ AUTHOR INFORMATION

Corresponding Authors

*E-mail: jodie.lutkenhaus@tamu.edu (J.L.).
*E-mail: r_kostecki@lbl.gov (R.K.).
*E-mail: rafaelv@rice.edu (R.V.).

ORCID

Atetegeb Meazah Haregewoin: 0000-0003-4272-3760
Jodie Lutkenhaus: 0000-0002-2613-6016
Rafael Verduzco: 0000-0002-3649-3455

Author Contributions

The manuscript was written through contributions of all authors. All authors have given approval to the final version of the manuscript.

Notes

The authors declare no competing financial interest.

■ ACKNOWLEDGMENTS

We acknowledge the Support of the National Science Foundation under CBET−1604666 and 1604682, as well as the Welch Foundation for Chemical Research C-1888. This project was supported by the U.S. Department of Energy, Office of Science, Office of Workforce Development for Teachers and Scientists, and Office of Science Graduate Student Research (SCGSR) program. The SCGSR program is administered by the Oak Ridge Institute for Science and Education for the DOE under contract number DE-SC0014664. This work was also supported by the Assistant Secretary for Energy Efficiency and Renewable Energy, Office of Vehicle Technologies of the U.S. Department of Energy under Contract No. DE-AC02-05CH11231, under the Applied Battery Research for Transportation (ABR) Program and Award Number DE-EE0006443. The authors thank Maura Puerto (Rice) for providing Flopaam powder.

■ ABBREVIATIONS

HPAM, hydrolyzed polyacrylamide

■ REFERENCES

(1) Dunn, J. B.; Gaines, L.; Barnes, M.; Sullivan, J. L.; Wang, M. *Material and Energy Flows in the Materials Production, Assembly, and End-of-Life Stages of the Automotive Lithium-Ion Battery Life Cycle*; Argonne National Lab (ANL): Argonne, IL, 2014.

(2) Feng, K.; Li, M.; Liu, W.; Kashkooli, A. G.; Xiao, X.; Cai, M.; Chen, Z. Silicon-Based Anodes for Lithium-Ion Batteries: From Fundamentals to Practical Applications. *Small* **2018**, *14*, No. 1702737.

(3) Veith, G. M.; Doucet, M.; Sacci, R. L.; Vacaliuc, B.; Baldwin, J. K.; Browning, J. F. Determination of the Solid Electrolyte Interphase Structure Grown on a Silicon Electrode Using a Fluoroethylene Carbonate Additive. *Sci. Rep.* **2017**, *7*, No. 6326.

(4) Zhao, H.; Yuan, W.; Liu, G. Hierarchical Electrode Design of High-Capacity Alloy Nanomaterials for Lithium-Ion Batteries. *Nano Today* **2015**, *10*, 193−212.

(5) Mazouzi, D.; Karkar, Z.; Reale Hernandez, C.; Jimenez Manero, P.; Guyomard, D.; Roué, L.; Lestriez, B. Critical Roles of Binders and Formulation at Multiscales of Silicon-Based Composite Electrodes. *J. Power Sources* **2015**, *280*, 533−549.

(6) Choi, N.-S.; Ha, S.-Y.; Lee, Y.; Jang, J. Y.; Jeong, M.-H.; Shin, W. C.; Ue, M. Recent Progress on Polymeric Binders for Silicon Anodes in Lithium-Ion Batteries. *J. Electrochem. Sci. Technol.* **2015**, *6*, 35−49.

(7) Huang, S.; Ren, J.; Liu, R.; Yue, M.; Huang, Y.; Yuan, G. The Progress of Novel Binder as a Non-ignorable Part to Improve the Performance of Si-based Anodes for Li-ion Batteries. *Int. J. Energy Res.* **2018**, *42*, 919−935.

(8) Kwon, T.; Choi, J. W.; Coskun, A. The Emerging Era of Supramolecular Polymeric Binders in Silicon Anodes. *Chem. Soc. Rev.* **2018**, *47*, 2145−2164.

(9) Kovalenko, I.; Zdyrko, B.; Magasinski, A.; Hertzberg, B.; Milicev, Z.; Burtovyy, R.; Luzinov, I.; Yushin, G. A Major Constituent of Brown Algae for Use in High-Capacity Li-Ion Batteries. *Science* **2011**, *334*, 75−79.

(10) Yoon, J.; Oh, D. X.; Jo, C.; Lee, J.; Hwang, D. S. Improvement of Desolvation and Resilience of Alginate Binders for Si-Based Anodes in a Lithium Ion Battery by Calcium-Mediated Cross-Linking. *Phys. Chem. Chem. Phys.* **2014**, *16*, 25628−25635.

(11) Magasinski, A.; Zdyrko, B.; Kovalenko, I.; Hertzberg, B.; Burtovyy, R.; Huebner, C. F.; Fuller, T. F.; Luzinov, I.; Yushin, G. Toward Efficient Binders for Li-Ion Battery Si-Based Anodes: Polyacrylic Acid. *ACS Appl. Mater. Interfaces* **2010**, *2*, 3004−3010.

(12) Wu, M.; Xiao, X.; Vukmirovic, N.; Xun, S.; Das, P. K.; Song, X.; Olalde-Velasco, P.; Wang, D.; Weber, A. Z.; Wang, L.-W.; et al. Toward an Ideal Polymer Binder Design for High-Capacity Battery Anodes. *J. Am. Chem. Soc.* **2013**, *135*, 12048−12056.

(13) Zhu, X.; Zhang, F.; Zhang, L.; Zhang, L.; Song, Y.; Jiang, T.; Sayed, S.; Lu, C.; Wang, X.; Sun, J.; et al. A Highly Stretchable Cross-Linked Polyacrylamide Hydrogel as an Effective Binder for Silicon and Sulfur Electrodes toward Durable Lithium-Ion Storage. *Adv. Funct. Mater.* **2018**, *28*, No. 1705015.

(14) Yoo, J.-K.; Jeon, J.; Kang, K.; Jung, Y. S. Glyoxalated Polyacrylamide as a Covalently Attachable and Rapidly Cross-Linkable Binder for Si Electrode in Lithium Ion Batteries. *Electron. Mater. Lett.* **2017**, *13*, 136−141.

(15) Lucas, E. F.; Mansur, C. R. E.; Spinelli, L.; Queirós, Y. G. C. Polymer Science Applied to Petroleum Production. *Pure Appl. Chem.* **2009**, *81*, 473−494.

(16) Wever, D. A. Z.; Picchioni, F.; Broekhuis, A. A. Polymers for Enhanced Oil Recovery: A Paradigm for Structure−Property Relationship in Aqueous Solution. *Prog. Polym. Sci.* **2011**, *36*, 1558−1628.

(17) Karkar, Z.; Guyomard, D.; Roué, L.; Lestriez, B. A Comparative Study of Polyacrylic Acid (PAA) and Carboxymethyl Cellulose (CMC) Binders for Si-Based Electrodes. *Electrochim. Acta* **2017**, *258*, 453−466.

(18) Qiao, H.-B.; Tian, X.-M.; Yi, T.-F. Electrochemical Properties of Si Negative Electrodes Bonded with Partially Hydrolyzed Polyacrylamide for Li-Ion Batteries. *Int. J. Electrochem. Sci.* **2013**, *8*, 9414.

(19) Haregewoin, A. M.; Terborg, L.; Zhang, L.; Jurng, S.; Lucht, B. L.; Guo, J.; Ross, P. N.; Kostecki, R. The Electrochemical Behavior of Poly 1-Pyrenemethyl Methacrylate Binder and Its Effect on the

Interfacial Chemistry of a Silicon Electrode. *J. Power Sources* **2018**, *376*, 152−160.
(20) Zhao, H.; Wei, Y.; Wang, C.; Qiao, R.; Yang, W.; Messersmith, P. B.; Liu, G. Mussel-Inspired Conductive Polymer Binder for Si-Alloy Anode in Lithium-Ion Batteries. *ACS Appl. Mater. Interfaces* **2018**, *10*, 5440−5446.
(21) Chen, Z.; Christensen, L.; Dahn, J. R. Large-Volume-Change Electrodes for Li-Ion Batteries of Amorphous Alloy Particles Held by Elastomeric Tethers. *Electrochem. Commun.* **2003**, *5*, 919−923.
(22) Ryou, M.-H.; Kim, J.; Lee, I.; Kim, S.; Jeong, Y. K.; Hong, S.; Ryu, J. H.; Kim, T.-S.; Park, J.-K.; Lee, H.; et al. Mussel-Inspired Adhesive Binders for High-Performance Silicon Nanoparticle Anodes in Lithium-Ion Batteries. *Adv. Mater.* **2013**, *25*, 1571−1576.
(23) Jeong, Y. K.; Kwon, T.; Lee, I.; Kim, T.-S.; Coskun, A.; Choi, J. W. Hyperbranched β-Cyclodextrin Polymer as an Effective Multi-dimensional Binder for Silicon Anodes in Lithium Rechargeable Batteries. *Nano Lett.* **2014**, *14*, 864−870.
(24) Liu, W.-R.; Yang, M.-H.; Wu, H.-C.; Chiao, S. M.; Wu, N.-L. Enhanced Cycle Life of Si Anode for Li-Ion Batteries by Using Modified Elastomeric Binder. *Electrochem. Solid-State Lett.* **2005**, *8*, A100−A103.
(25) Zhao, H.; Wei, Y.; Qiao, R.; Zhu, C.; Zheng, Z.; Ling, M.; Jia, Z.; Bai, Y.; Fu, Y.; Lei, J.; et al. Conductive Polymer Binder for High-Tap-Density Nanosilicon Material for Lithium-Ion Battery Negative Electrode Application. *Nano Lett.* **2015**, *15*, 7927−7932.
(26) Yim, T.; Choi, S. J.; Jo, Y. N.; Kim, T.-H.; Kim, K. J.; Jeong, G.; Kim, Y.-J. Effect of Binder Properties on Electrochemical Performance for Silicon-Graphite Anode: Method and Application of Binder Screening. *Electrochim. Acta* **2014**, *136*, 112−120.
(27) Vogl, U. S.; Das, P. K.; Weber, A. Z.; Winter, M.; Kostecki, R.; Lux, S. F. Mechanism of Interactions between CMC Binder and Si Single Crystal Facets. *Langmuir* **2014**, *30*, 10299−10307.
(28) Uchida, S.; Mihashi, M.; Yamagata, M.; Ishikawa, M. Electrochemical Properties of Non-Nano-Silicon Negative Electrodes Prepared with a Polyimide Binder. *J. Power Sources* **2015**, *273*, 118−122.
(29) Guo, S.; Li, H.; Li, Y.; Han, Y.; Chen, K.; Xu, G.; Zhu, Y.; Hu, X. SiO2-Enhanced Structural Stability and Strong Adhesion with a New Binder of Konjac Glucomannan Enables Stable Cycling of Silicon Anodes for Lithium-Ion Batteries. *Adv. Energy Mater.* **2018**, *8*, No. 1800434.
(30) Choi, J.; Kim, K.; Jeong, J.; Cho, K. Y.; Ryou, M.-H.; Lee, Y. M. Highly Adhesive and Soluble Copolyimide Binder: Improving the Long-Term Cycle Life of Silicon Anodes in Lithium-Ion Batteries. *ACS Appl. Mater. Interfaces* **2015**, *7*, 14851−14858.
(31) Nguyen, B. P. N.; Chazelle, S.; Cerbelaud, M.; Porcher, W.; Lestriez, B. Manufacturing of Industry-Relevant Silicon Negative Composite Electrodes for Lithium Ion-Cells. *J. Power Sources* **2014**, *262*, 112−122.
(32) Stafford, C. M.; Roskov, K. E.; Epps, T. H., III; Fasolka, M. J. Generating Thickness Gradients of Thin Polymer Films via Flow Coating. *Rev. Sci. Instrum.* **2006**, *77*, No. 023908.
(33) Thurber, W. R. Resistivity-Dopant Density Relationship for Boron-Doped Silicon. *J. Electrochem. Soc.* **1980**, *127*, 2291.
(34) Park, S.-J.; Zhao, H.; Ai, G.; Wang, C.; Song, X.; Yuca, N.; Battaglia, V. S.; Yang, W.; Liu, G. Side-Chain Conducting and Phase-Separated Polymeric Binders for High-Performance Silicon Anodes in Lithium-Ion Batteries. *J. Am. Chem. Soc.* **2015**, *137*, 2565−2571.
(35) Jenkins, C. L.; Meredith, H. J.; Wilker, J. J. Molecular Weight Effects upon the Adhesive Bonding of a Mussel Mimetic Polymer. *ACS Appl. Mater. Interfaces* **2013**, *5*, 5091−5096.
(36) Kwon, T.; Jeong, Y. K.; Lee, I.; Kim, T.-S.; Choi, J. W.; Coskun, A. Systematic Molecular-Level Design of Binders Incorporating Meldrum's Acid for Silicon Anodes in Lithium Rechargeable Batteries. *Adv. Mater.* **2014**, *26*, 7979−7985.
(37) Porcher, W.; Chazelle, S.; Boulineau, A.; Mariage, N.; Alper, J. P.; Rompaey, T. V.; Bridel, J.-S.; Haon, C. Understanding Polyacrylic Acid and Lithium Polyacrylate Binder Behavior in Silicon Based Electrodes for Li-Ion Batteries. *J. Electrochem. Soc.* **2017**, *164*, A3633−A3640.
(38) Lu, X.; Mi, Y. Characterization of the Interfacial Interaction between Polyacrylamide and Silicon Substrate by Fourier Transform Infrared Spectroscopy. *Macromolecules* **2005**, *38*, 839−843.
(39) Vogl, U. S.; Lux, S. F.; Crumlin, E. J.; Liu, Z.; Terborg, L.; Winter, M.; Kostecki, R. The Mechanism of SEI Formation on a Single Crystal Si(100) Electrode. *J. Electrochem. Soc.* **2015**, *162*, A603−A607.
(40) Xu, C.; Lindgren, F.; Philippe, B.; Gorgoi, M.; Björefors, F.; Edström, K.; Gustafsson, T. Improved Performance of the Silicon Anode for Li-Ion Batteries: Understanding the Surface Modification Mechanism of Fluoroethylene Carbonate as an Effective Electrolyte Additive. *Chem. Mater.* **2015**, *27*, 2591−2599.
(41) Jin, Y.; Zhu, B.; Lu, Z.; Liu, N.; Zhu, J. Challenges and Recent Progress in the Development of Si Anodes for Lithium-Ion Battery. *Adv. Energy Mater.* **2017**, *7*, No. 1700715.
(42) Shi, F.; Song, Z.; Ross, P. N.; Somorjai, G. A.; Ritchie, R. O.; Komvopoulos, K. Failure Mechanisms of Single-Crystal Silicon Electrodes in Lithium-Ion Batteries. *Nat. Commun.* **2016**, *7*, No. 11886.
(43) Ma, D.; Cao, Z.; Hu, A. Si-Based Anode Materials for Li-Ion Batteries: A Mini Review. *Nano-Micro Lett.* **2014**, *6*, 347−358.
(44) Lee, K.-L.; Jung, J.-Y.; Lee, S.-W.; Moon, H.-S.; Park, J.-W. Electrochemical Characteristics of A-Si Thin Film Anode for Li-Ion Rechargeable Batteries. *J. Power Sources* **2004**, *129*, 270−274.
(45) Li, H.; Huang, X.; Chen, L.; Wu, Z.; Liang, Y. A High Capacity Nano - Si Composite Anode Material for Lithium Rechargeable Batteries. *Electrochem. Solid-State Lett.* **1999**, *2*, 547−549.
(46) Nguyen, C. C.; Yoon, T.; Seo, D. M.; Guduru, P.; Lucht, B. L. Systematic Investigation of Binders for Silicon Anodes: Interactions of Binder with Silicon Particles and Electrolytes and Effects of Binders on Solid Electrolyte Interphase Formation. *ACS Appl. Mater. Interfaces* **2016**, *8*, 12211−12220.
(47) Brooks, D. J.; Merinov, B. V.; Goddard, W. A.; Kozinsky, B.; Mailoa, J. Atomistic Description of Ionic Diffusion in PEO−LiTFSI: Effect of Temperature, Molecular Weight, and Ionic Concentration. *Macromolecules* **2018**, *51*, 8987−8995.
(48) Kasinathan, R.; Marinaro, M.; Axmann, P.; Wohlfahrt-Mehrens, M. Influence of the Molecular Weight of Poly-Acrylic Acid Binder on Performance of Si-Alloy/Graphite Composite Anodes for Lithium-Ion Batteries. *Energy Technol.* **2018**, *6*, 2256−2263.
(49) Lee, B.-R.; Oh, E.-S. Effect of Molecular Weight and Degree of Substitution of a Sodium-Carboxymethyl Cellulose Binder on Li4Ti5O12 Anodic Performance. *J. Phys. Chem. C* **2013**, *117*, 4404−4409.
(50) Philippe, B.; Dedryvère, R.; Allouche, J.; Lindgren, F.; Gorgoi, M.; Rensmo, H.; Gonbeau, D.; Edström, K. Nanosilicon Electrodes for Lithium-Ion Batteries: Interfacial Mechanisms Studied by Hard and Soft X-Ray Photoelectron Spectroscopy. *Chem. Mater.* **2012**, *24*, 1107−1115.
(51) Bresser, D.; Buchholz, D.; Moretti, A.; Varzi, A.; Passerini, S. Alternative Binders for Sustainable Electrochemical Energy Storage − the Transition to Aqueous Electrode Processing and Bio-Derived Polymers. *Energy Environ. Sci.* **2018**, *11*, 3096−3127.
(52) Chen, H.; Ling, M.; Hencz, L.; Ling, H. Y.; Li, G.; Lin, Z.; Liu, G.; Zhang, S. Exploring Chemical, Mechanical, and Electrical Functionalities of Binders for Advanced Energy-Storage Devices. *Chem. Rev.* **2018**, *118*, 8936−8982.
(53) Bie, Y.; Yang, J.; Nuli, Y.; Wang, J. Natural Karaya Gum as an Excellent Binder for Silicon-Based Anodes in High-Performance Lithium-Ion Batteries. *J. Mater. Chem. A* **2017**, *5*, 1919−1924.
(54) Lopez, J.; Chen, Z.; Wang, C.; Andrews, S. C.; Cui, Y.; Bao, Z. The Effects of Cross-Linking in a Supramolecular Binder on Cycle Life in Silicon Microparticle Anodes. *ACS Appl. Mater. Interfaces* **2016**, *8*, 2318−2324.
(55) Li, P.; Zhao, G.; Zheng, X.; Xu, X.; Yao, C.; Sun, W.; Dou, S. X. Recent Progress on Silicon-Based Anode Materials for Practical

Lithium-Ion Battery Applications. *Energy Storage Mater.* **2018**, *15*, 422−446.
(56) Shi, Y.; Zhou, X.; Yu, G. Material and Structural Design of Novel Binder Systems for High-Energy, High-Power Lithium-Ion Batteries. *Acc. Chem. Res.* **2017**, *50*, 2642−2652.
(57) Lestriez, B. Functions of Polymers in Composite Electrodes of Lithium Ion Batteries. *C. R. Chim.* **2010**, *13*, 1341−1350.
(58) Yue, L.; Zhang, L.; Zhong, H. Carboxymethyl Chitosan: A New Water Soluble Binder for Si Anode of Li-Ion Batteries. *J. Power Sources* **2014**, *247*, 327−331.
(59) Ryu, J. H.; Kim, J. W.; Sung, Y.-E.; Oh, S. M. Failure Modes of Silicon Powder Negative Electrode in Lithium Secondary Batteries. *Electrochem. Solid-State Lett.* **2004**, *7*, A306−A309.
(60) Park, C.-M.; Kim, J.-H.; Kim, H.; Sohn, H.-J. Li-Alloy Based Anode Materials for Li Secondary Batteries. *Chem. Soc. Rev.* **2010**, *39*, 3115−3141.
(61) Wu, H.; Cui, Y. Designing Nanostructured Si Anodes for High Energy Lithium Ion Batteries. *Nano Today* **2012**, *7*, 414−429.